JOURNAL OF GEOPHYSICAL RESEARCH, VOL. 113, E00A20, doi:10.1029/2007JE003034, 2008

Expected atmospheric environment for the Phoenix landing season and location

Leslie K. Tamppari,[1] Jeffrey Barnes,[2] Eugene Bonfiglio,[1] Bruce Cantor,[3] A. James Friedson,[1] Amitabha Ghosh,[4] M. Rob Grover,[1] David Kass,[1] Terry Z. Martin,[1] Michael Mellon,[5] Tim Michaels,[6] Jim Murphy,[7] Scot C. R. Rafkin,[6] Michael D. Smith,[8] Glenn Tsuyuki,[1] Daniel Tyler Jr.,[2] and Michael Wolff[9]

Received 1 November 2007; revised 3 March 2008; accepted 29 May 2008; published 28 October 2008.

[1] The Phoenix mission, launched on 4 August 2007, landed in the far northern plains of Mars on 25 May 2008. In order to prepare for the landing events and the 90-sol mission, a significant amount of work has gone into characterizing the atmospheric environment at this location on Mars for northern late spring through midsummer. In this paper we describe the motivation for the work and present our results on atmospheric densities and winds expected during the Phoenix entry, descent, and landing, as well as near-surface pressure, temperature, winds, surface temperature, and visible optical depth expected over the course of the science mission.

Citation: Tamppari, L. K., et al. (2008), Expected atmospheric environment for the Phoenix landing season and location, *J. Geophys. Res.*, *113*, E00A20, doi:10.1029/2007JE003034.

1. Introduction

[2] Throughout the course of the Phoenix mission development, a significant amount of work has been done to understand the atmospheric environment expected in the Phoenix landing latitude zone and during the mission. This work was needed to ensure a safe landing of the Phoenix spacecraft, to ensure that the spacecraft will operate as desired under the expected range of conditions while on the surface, and to allow the science observations to be planned appropriately.

[3] During the entry, decent, and landing (EDL) through the atmosphere, Phoenix will decelerate owing to the atmospheric density. At about 16 km altitude, Phoenix will deploy a parachute, further reducing the velocity. At this altitude and below, winds become important as they may affect the motion of the spacecraft on the parachute and the measurements of the descent radar, which is used to measure altimetry and velocity. At about 1 km above the surface, Phoenix will turn on powered-descent engines to stabilize and slow the spacecraft to a soft landing. Phoenix will also land at 1620 local mean solar time, a time for which the boundary layer is expected to still be quite active. Because the spacecraft will respond to density and winds in the atmosphere, estimates of these quantities were critical to enable the engineering team to design the EDL process to withstand the range of conditions expected and land the Phoenix spacecraft safely.

[4] The Phoenix spacecraft is a stationary, solar-powered lander intended for an arctic landing site, but originally built for an equatorial landing site. Its heritage is the Mars Surveyor Program '01 (MSP'01) Lander and some instruments, which were nearly complete and into their test phase when the program was cancelled owing to the loss of the lander's sister spacecraft, the Mars Polar Lander (MPL) in 1999. Some of the instruments from MPL also provide heritage to the Phoenix instruments. The Phoenix mission, the first of a program of competed, cost-capped Mars missions called the Mars Scout program, proposed to re-use the partially built MSP'01 spacecraft, which helped lower overall mission costs. However, using a spacecraft and some instruments, originally intended to land at an equatorial site, to land in a polar site challenged the team to understand the environmental conditions expected and optimize where possible to provide the best science mission, all while maintaining a strong focus on cost. Environmental conditions such as winds and temperature affect the thermal state of the spacecraft and optical depth affects the amount of power generated by the solar panels as well as the thermal environment. A key concern at high latitudes, where temperatures are colder and the sun does not get as high in the sky, are dust storms that may block a significant amount of sunlight for multiple days. For these reasons, estimates of the surface pressure, near-surface winds, near-surface temperatures, optical depth, and frequency of dust storms throughout the mission were provided to the engineering team. This

[1]Jet Propulsion Laboratory, California Institute of Technology, Pasadena, California, USA.
[2]College of Oceanic and Atmospheric Sciences, Oregon State University, Corvallis, Oregon, USA.
[3]Malin Space Science Systems, Inc., San Diego, California, USA.
[4]Tharsis Inc., Gaithersburg, Maryland, USA.
[5]Laboratory for Atmospheric and Space Physics, University of Colorado, Boulder, Colorado, USA.
[6]Southwest Research Institute, Boulder, Colorado, USA.
[7]Department of Astronomy, New Mexico State University, Las Cruces, New Mexico, USA.
[8]Goddard Space Flight Center, Greenbelt, Maryland, USA.
[9]Space Science Institute, Boulder, Colorado, USA.

0148-0227/08/2007JE003034$09.00

allowed them to perform analyses and tests of and optimize the design where possible for the spacecraft thermal and power systems and for the payload.

[5] Phoenix was launched on 4 August 2007 and will arrive on the northern plains of Mars on 25 May 2008 which corresponds to L_s = 76, in the late northern spring. The primary mission of 90 sols (1 Martian day = 1 sol = 24.7 Earth hours) will mean that the Phoenix spacecraft will be operating through L_s = 117 or midnorthern summer. The landing location will be approximately 68.2N/126.6W in a safe valley within the Scandia formation in the northern plains of Mars (Figure 1; see *Arvidson et al.* [2008] for more information on the landing region). The exact landing location is uncertain owing to uncertainty in the exact entry point of the spacecraft into the atmosphere and the effect of the atmosphere on the EDL trajectory. This uncertainty creates a probability ellipse that is approximately 150 km long by 30 km wide.

[6] At the landing season, the CO_2 and water frost that covers this high northern latitude during winter will have receded and the ground will have warmed. The polar hood will have receded as well, but off-cap dust storms may still reach the landing latitude. As the mission progresses, both water-ice and dust optical depths should decrease. Water vapor, on the other hand, will be increasing to a peak near Ls = 110 owing to the seasonal cap sublimation. The environment at the landing site may also be influenced by Alba Patera, to the south, and the spacecraft may experience nighttime drainage winds or other synoptic winds associated with that topographic rise.

[7] In order to provide the necessary atmospheric input for EDL, a working group consisting of atmospheric scientists and EDL engineers was formed. The charter of this group was to model and understand the atmospheric environment at the landing location and season, to understand the sensitivities of the spacecraft system to atmospheric density and winds, and to provide estimates of these quantities that included the expected conditions plus variability and uncertainty. Section 2 discusses the details of this process. Two modeling groups provided Mesoscale model and Large Eddy Simulation (LES) output: Oregon State University (OSU) and Southwest Research Institute (SwRI). The models generated by these two groups are described and discussed in sections 2.2 and 2.3, respectively. The spacecraft sensitivities to winds and density are described in section 2.4. Model output combined with data, when available, was used to provide sets of 2000 atmospheric density or wind profiles suitable for use by the engineering team and these processes are discussed in sections 2.5 and 2.6. Finally, section 2.7 discusses the results of spacecraft simulations through these modeled atmospheric profiles.

[8] Information required for surface operations is discussed in section 3, with a description of what quantities were needed and why given in section 3.1. Surface pressure estimates, bounded for the variety of landing locations initially studied plus uncertainties associated with storms, are discussed in section 3.2. Section 3.3 provides our estimates of the total visible optical depth, including both water-ice and dust contributions throughout the mission lifetime, as well as the frequency and expected maximum optical depth of potential dust storms. Section 3.4 discusses our estimates of surface winds and section 3.5 discusses the estimated near-surface and surface temperatures.

[9] The estimated atmospheric quantities, both for EDL and for surface operations, were peer reviewed during the course of the mission development. The peer review team consisted of Mars atmospheric scientists with expertise in circulation modeling as well as expertise in current Mars atmospheric data sets. In addition, several members of the engineering community with experience in a similar process used for the Mars Exploration Rovers also served as review board members.

2. Atmospheric Information Required for Entry, Descent, and Landing

2.1. Overview

[10] A spacecraft must be designed and optimized to autonomously fly through the atmosphere and land safely on the surface. As such, it must be able to withstand the winds and wind shears predicted for the landing location and season. Since there are few measurements of these quantities on Mars, the spacecraft engineering team relied on modeled predictions of these winds. The density and density variability expected in the atmosphere must also be estimated and the spacecraft must be able to fly safely through it. Densities are estimated on the basis of data and model output.

[11] Over the course of the Phoenix mission development, we prepared 9 total mesoscale model runs between the OSU and SwRI groups. These models both included larger/coarser grids encompassing a large portion of the north polar region, as well as smaller/finer grids nested over the Phoenix regions of interest. The models used a variety of polar cap prescriptions, which drove storms differently and allowed us to see the potential range of possibilities the spacecraft might experience. We also investigated the effects of dust loading in the atmosphere. We investigated the effect of variable optical depth as a function of latitude and seasonal date with specification of different amounts of dust at the Phoenix site, ranging from τ_{vis} = 0.05 to 0.5. Furthermore, we investigated the effect of dust distribution with height in the atmosphere, using as a guide the Mars Global Surveyor (MGS) Thermal Emission Spectrometer (TES) limb profiles [*Christensen et al.*, 1992; *Smith*, 2003], to investigate the effect on the strength and location of the polar jet. We found that while the jet was strengthened, there was little effect in the winds at latitudes as far south as the Phoenix landing location. Finally, we investigated the effects of active dust lifting. In all these simulations, winds at the Phoenix landing site were typically <20 m/s between 1 and 40 km altitude and the spacecraft is thought to begin to encounter problems only when winds are greater than 30 m/s.

[12] In order to resolve higher-resolution winds and to better understand motions in the boundary layer, which are parameterized in mesoscale models, a total of 9 large eddy simulations were also performed between the two groups. These were run for a typical grid spacing of 100 m in the horizontal and vertical and over 20 square km area. The two models produced slightly different heights for the top of the boundary layer ($\sim$7 km for OSU and $\sim$5 km for SwRI). For these simulations, we varied the surface thermal inertia and

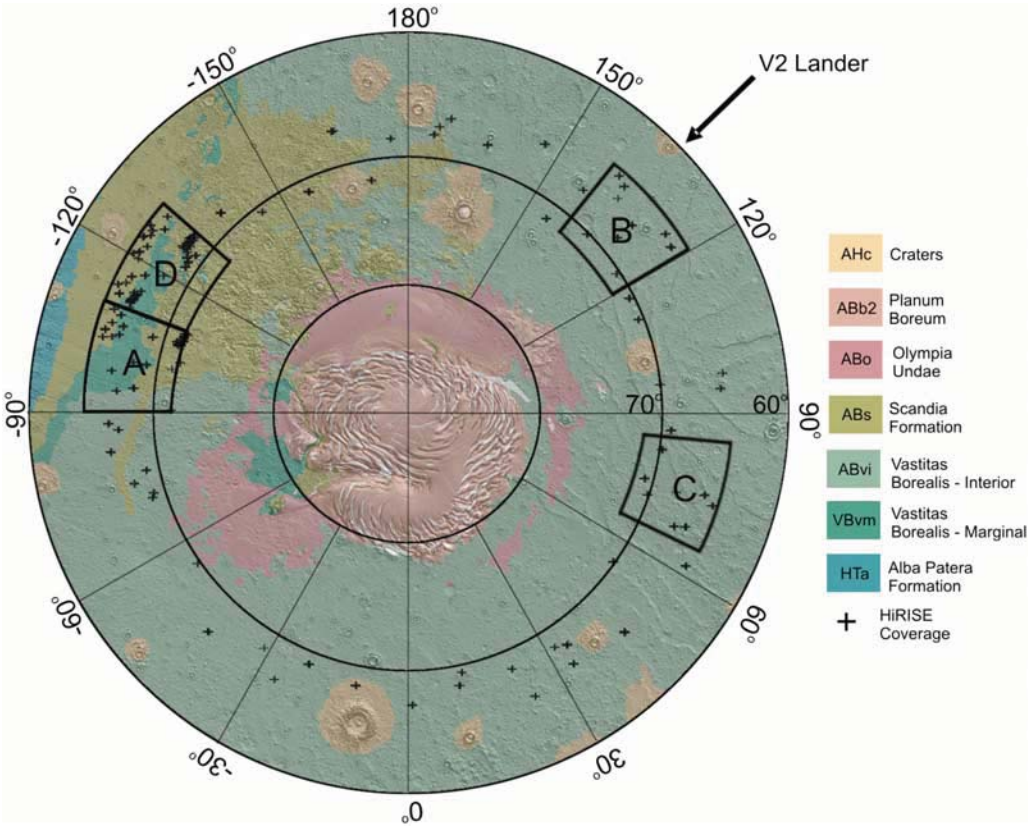

Figure 1. The Phoenix landing location at ~68.2N/126.6W is shown in region D. Other regions shown were considered prior to selection of region D. The crosses represent images taken by MRO HiRISE in support of Phoenix landing site selection.

albedo values and ultimately selected values that were representative of the driving case for the Phoenix landing site. We also investigated the effect of constant low-speed (2–5 m/s) and high-speed (15 m/s) background winds, as well as a time and height varying background winds. When the background winds are strong, shear production appears to dominate over buoyancy. Both the mesoscale and LES models are described in more detail in sections 2.2 and 2.3 below.

[13] Section 2.4 discusses the spacecraft sensitivities to atmospheric density and winds, as well as the Monte Carlo analyses performed by the engineering team. In these analyses, the spacecraft is "flown" through the set of 2000 density and wind profiles and statistics are gathered to understand and reveal any potential vulnerabilities in the entry, descent and landing of the Phoenix spacecraft.

[14] Three techniques were used to provide wind profiles to the EDL engineering team; we provided 8 sets of 2000 profiles. One was similar to the process followed for the Mars Exploration Rovers [*Golombek et al.*, 2003] that made use of the Turbulent Kinetic Energy produced in the SwRI mesoscale model. The energy represented by the TKE was apportioned to all scales, down to about 10 m, according to a power spectrum with a −5/3 slope. The second technique used the LES output directly up to about 10 km altitude and then merged that with the mesoscale output at higher altitudes. In both cases, 10% "outlier" profiles with larger horizontal winds, often from near-polar cap storms, were added to the wind profile set provided. We confirmed that the spatial spectrum of small-scale winds created by the TKE model was accurate by analyzing against the LES model. In addition, we confirmed that the spectral slope used in the TKE model agrees with Earth boundary layer observations [*Kaimal et al.*, 1972; *Caughey and Wyngaard*, 1979]. The third technique was to use the TKE output produced by the OSU LES as input to the power spectral model for wind profile production. These techniques are discussed in detail in section 2.5.

[15] Over the course of the development of the Phoenix mission we also provided density profile sets to the engineering team: 4 separate deliveries. Each set contains MGS TES data from the Phoenix latitude annulus (65–72N). Between December 2005 and October 2006, prior to the Mars Reconnaissance Orbiter (MRO) High Resolution Imaging Science Experiment (HiRISE) [*McEwen et al.*, 2007] camera imaging, the Phoenix team had downselected to region B (120–140E; see Figure 1). The region had mean elevations of ~−4000 m with respect to the Mars Orbiter Laser Altimeter (MOLA; *Zuber et al.* [1992]) geoid, so we provided density profiles that were constrained in elevation to −4000 m ± 400 m. After receiving the first HiRISE images of region B, we quickly realized, owing to the widespread, ubiquitous boulder fields, that we would have to find a safer place to land [see also *Arvidson et al.*, 2008]. After finding that region D provided several safe landing locations, we updated our density profile sets to elevations more representative of this region in general, −3700 m ± 300 m. The method used to produce these data

sets is described in section 2.6. Finally, section 2.7 covers preliminary results of the EDL simulations.

2.2. The Oregon State University Mars Mesoscale Model 5 and Mars Large Eddy Simulation Models and Model Simulations

[16] The Oregon State University Mars Atmospheric Modeling Group has used its toolbox of atmospheric computer models to constrain the range of meteorology that Phoenix might encounter during EDL and on the surface during the primary mission. These models are the OSU MMM5 model [*Tyler et al.*, 2002; *Tyler and Barnes*, 2005] and the OSU MLES model [*Tyler and Barnes*, 2006]. Design of these experiments and the results (as briefly described in this section) are presented in much greater detail in a companion manuscript in this special edition [*Tyler et al.*, 2008].

2.2.1. Mesoscale Model Simulations

[17] The OSU mesoscale model is run on a semiglobal polar-stereographic mother domain that reaches into the southern hemisphere. Two-way nesting is used recursively to reach the highest resolutions (generally 18 km, although some simulations also had 6 km nests). The vertical grid of the model maintains high resolution below ~5–10 km, becoming coarse to the model top at ~45 km (a total of 32 layers, the center of the lowest layer is ~1.7 m). The model is run for 29 sols and the first 9 sols are discarded to spin-up. A version of the NASA Ames Mars Global Circulation Model (GCM) [*Haberle et al.*, 1999], which is maintained at OSU, provides initial and hourly boundary conditions. The final 20 sols of each simulation provide guidance and are processed into relevant statistics about the prominent transient eddy circulations (storms) that are seen in model results. An extensive spin-up period is required so the model has completely adjusted to all of the following: the polar-stereographic grid, the higher-resolution surface fields (topography, albedo and thermal inertia) and the important thermal forcing of the seasonal cap, which is prescribed in accordance with MGS/TES ground temperatures (M. D. Smith, personal communication, 2006) and the visible and thermal boundaries of the remaining seasonal cap (J. Benson, personal communication, 2004; see also *Titus* [2005]). Moreover, the GCM initial conditions do not resolve the transient circulations; thus, spin-up time is needed for these storms to form and establish their importance in the polar atmosphere.

[18] Because temperatures within the seasonal cap are constantly cold, there is a discontinuity in the meridional gradient of ground temperature. This causes a gradient in atmospheric temperatures and a jet forms in the zonal wind. In the OSU MMM5 the zonal-mean jet forms above the edge of the zonal mean seasonal cap at ~80–85°N, with a jet-max of ~20 m/s at an altitude of ~10 km above ground level (AGL). The amplitude of the jet-max is very sensitive to the configuration of the model, most specifically the prescription for the seasonal cap and the opacity of atmospheric dust. Model sensitivity studies suggest that the synoptic structure of storms that form along this jet is in seasonal transition when Phoenix arrives; it is transitioning from a wave number-two structure (dominant shortly before the L_s of EDL with storms progressing with the jet around the seasonal cap) to a wave number-one structure with retrograde storm motion (seen by *Tyler and Barnes* [2005] in their study of northern summertime polar circulations). Since numerical weather prediction for Mars is not presently available, the best guidance concerning these storms is a statistical analysis of their strength and influence on local meteorology as a function of latitude. Almost without exception, the effect of these storms on the local meteorology is within engineering tolerances (wind profiles poleward of ~75°N can be too strong, but the Phoenix spacecraft will land at ~68°N).

2.2.2. Large Eddy Simulations

[19] The OSU MLES model is used to provide explicit simulation of the variability in horizontal and vertical winds that would be expected owing to turbulent convection at the time of EDL, which is about 1630 local mean solar time. This model is initialized with temperatures and surface properties taken from an OSU MMM5 simulation for a specific time and location. For these Phoenix studies the OSU MLES was run with a spatially uniform resolution of 100 m on a large and deep domain (30 km × 30 km × 25 km). Geostrophic wind is a tunable model parameter; it can be constant or set to vary in both time and height. Analysis of mesoscale model results shows that constant geostrophic wind speeds of 5 m/s and 10 m/s are typical afternoon values for 70°N and 75°N throughout the profile, although the model was run with a range of wind speeds (2, 5, 10, and 15 m/s) to examine the sensitivity to this parameter. The model was also run with geostrophic wind forcing derived from the OSU MMM5 for a location near the southern point of the region A/D boundary. The mean winds in this simulation compare favorably with the mesoscale model, allowing us to see the turbulent structure that would exist with the presence of realistic synoptic forcing.

[20] Vertical velocity extrema are typically −10 and 15 m/s, showing that upward motions occur over smaller spatial areas than downward motions (the distribution is not Gaussian, but these extrema are well outside a $\pm 3\sigma$ envelope). Large downward velocities do occur very near the ground, whereas the largest upward velocities occur in the upper half of the mixed layer (at altitudes of ~3 km). The vertical velocity range is somewhat sensitive to two factors: (1) the geostrophic wind forcing and (2) the surface albedo; it widens somewhat with stronger wind forcing or decreased surface albedo. The horizontal mean turbulent kinetic energy (TKE) is sensitive to both wind shear and stability (sensitivity was explored by varying the wind forcing and the albedo). By late morning the convective structure transitions from being dominated by closed-cell convection to polygonal open-cell convection, with horizontal scales of ~3–5 km at 1.5 km above ground level (AGL) being dominant at the time of EDL. Maximum TKE values are ~10 m^2/s^2, typically seen at ~3 km, although if the wind is stronger such amplitudes also occur very near the ground, below ~500 m.

[21] At the local time of EDL, about 1620 Mars local mean solar time, horizontal winds very near the ground (below ~500 m) are very turbulent, with a range that is roughly twice that of the horizontal mean wind at the top of this layer (the superadiabatic layer). With significantly larger background wind speeds the convection does exhibit signs of having transitioned into a realm where convective rolls form, which can lead to larger turbulent excursions in a direction perpendicular to the wind vector (better than in the

direction of the wind). Depending upon the time it takes the spacecraft to respond to changes in the wind field, a 3-sigma combination of mean and turbulent winds (if encountered just prior to dropping from the parachute) give the greatest risk to the spacecraft, but horizontal and vertical velocities appear to still be within the envelope of engineering tolerances (for a more full description, see *Tyler et al.* [2008]).

[22] The simulated depth of the convective mixed layer in the OSU MLES is deeper than seen in the OSU MMM5 by ~1 km. The "top" of the turbulence is another ~1 km higher, ~7 km. Owing to storm driven interdiurnal variability of the wind and temperature profiles, the convective mixed layer will not grow uniformly every sol; a conservative estimate has the top of turbulence at ~8 km. Even with this very conservative estimate, the turbulence will be below the altitude where the parachute is deployed.

2.3. The Southwest Research Institute Mesoscale and LES Models and Model Results

[23] The modeling group at Southwest Research Institute (SwRI) utilized the Mars Regional Atmospheric Modeling System (MRAMS) [*Rafkin et al.*, 2001] to investigate the likely range of atmospheric conditions that the Phoenix mission might encounter. This model has been previously used to provide EDL planning support for the Mars Exploration Rover (MER) mission [*Rafkin and Michaels*, 2003] and to anticipate the atmospheric conditions that the Beagle 2 Lander would have experienced [*Rafkin et al.*, 2004]. MRAMS is a nonhydrostatic, fully compressible, limited-domain (i.e., not global) atmospheric model that can use a series of nested grids to model a location of interest at relatively high spatial resolution. In addition to its mesoscale (i.e., grid spacing of greater than about 500 m, but less than 0 (100 km)) capabilities, MRAMS may be used at spatial scales that qualify as a large eddy simulation (LES; for Mars, grid spacing typically <200 m) [*Michaels and Rafkin*, 2004].

2.3.1. SwRI MRAMS Simulations

[24] The MRAMS mesoscale simulations performed for the Phoenix mission primarily used nested north polar stereographic computational grids (see also *Michaels and Rafkin* [2008]). The coarsest of these grids encompassed more than an entire hemisphere, and the finest pole-centered grid had a nominal grid spacing that ranged from 17 km to 67 km (depending on the experiment). Some simulations also included grids centered on candidate landing regions that had a finer grid spacing of approximately 6 km. The vertical computational grid had 60 points, with a grid spacing nearest the surface of 15 m, then geometrically stretched to a maximum of 2.5 km aloft (total vertical depth of the model domain was approximately 70 km). The general mesoscale simulation procedure was to run with a static (no temporal evolution, phase change) polar cap for 10 to 20 sols. The polar cap extent used was that appropriate for the Phoenix landing season (L_s = 76).

[25] The mesoscale results exhibit a relatively weak polar vortex with peak core winds of less than 30 m/s. Transient baroclinic disturbances ("storms") are present in the model solution as well, primarily manifesting as a highly diurnally modulated "wave-2" structure with a rotational period (about the pole) of roughly 7 sols. Although these disturbances are primarily confined poleward of the northern boundary (72N) of the Phoenix landing site latitude range (65N–72N), they appear to occasionally affect the landing site regions. In general, the simulated environmental conditions within the targeted latitude band are found to be relatively homogeneous, with the slight exception of region A (see Figure 1), where there appears to be a relatively significant influence from the sizable topography to the south (Alba Patera and related areas of Tharsis) in the form of daily meridional flows that modulate transient baroclinic disturbances on a regional scale.

[26] The conditions within the Phoenix landing site latitude band were little affected in modeling experiments which varied the vertical depth of the prescribed dust loading in the polar region, although some cases produced relatively significant changes in the polar jet and other areas significantly to the north. Further modeling studies incorporating interactive dust (where radiatively active dust is injected into and transported by the atmosphere) exhibited no significantly enhanced wind speeds associated with the modeled dust plumes compared to the results with noninteractive dust. Further, the dust plumes appeared qualitatively similar to observed phenomena.

2.3.2. SwRI Large Eddy Simulations

[27] The MRAMS LES for the Phoenix mission were conducted using an isotropic grid with 200 × 200 × 101 points, with a grid spacing of 100 m. The computational domain size and grid spacing were chosen in order to resolve a statistically significant quantity of the largest convective cells within the afternoon convective boundary layer (CBL), while keeping the computational expense (i.e., computer processing time) at a practical level. In order to keep the computational grids of the MRAMS LES and the OSU LES as similar as possible for comparison purposes, a stretched vertical grid was not employed. The subgrid-scale turbulence parameterization used is a prognostic turbulent kinetic energy (TKE) scheme [see *Michaels and Rafkin*, 2004]. Each LES was initialized horizontally homogeneously with a single early morning appropriate thermodynamic profile (and its corresponding surface characteristics: albedo, thermal inertia, surface aerodynamic roughness length, surface and subsurface temperatures) taken from a mesoscale simulation. For simplicity, no topographic variation was prescribed. Every LES was then run for approximately 16 Mars hours to fully encompass the waxing and waning of vigorous convection within the CBL at the Phoenix EDL latitudes and season.

[28] The LES results indicate that the CBL environment throughout the range of local times for Phoenix EDL (approximately 1300 to 1700 LMST) is quite turbulent. This is not surprising, as the vast majority of the sunlit portions of Mars should experience conditions conducive to such convection. The LES indicates that large variances about the mean vertical and horizontal winds are to be expected. For example, at 3.5 km above the ground during the EDL local time range, modeled vertical velocities ranged from approximately −10 to 15 m s^{-1} and the horizontal wind speeds varied approximately ±10 m s^{-1} from a 15 m s^{-1} mean. Furthermore, from the perspective of a spacecraft descending (on a parachute, relatively slowly) through this environment, the most significant perturbations are not randomly distributed in time and space, but instead exhibit a pronounced structure. The expected range of vertical wind shear profiles and surface characteristics within the Phoenix

latitude band and EDL season is found to modulate the magnitude of the turbulent fluctuations, but not to change the nature of the convection significantly (i.e., the production/maintenance of turbulence remains dominated by buoyancy forces instead of by wind shear effects). The depth of the CBL during the EDL "window" appears to be difficult to narrowly constrain (due largely to uncertainties in wind shear and surface properties), but the MRAMS results suggest a range between 3 and 7 km. Although there are numerous relatively significant technical differences between MRAMS and the OSU LES model, a comparison of the solutions from the two models is favorable, suggesting that the general LES results are robust (at least within the assumptions and approximations made by this partially idealized LES procedure/technique).

2.4. Model Usage in EDL Simulation

[29] The entry, descent and landing for any Mars Lander mission provides significant engineering challenges. Part of the challenge is the difficulty and near impossibility of doing a full EDL system real-world flight test prior to executing the actual landing. Thus high-fidelity simulations are used to provide system performance assessments and system validation. Important in this process is the accurate representation of environmental conditions expected on Mars.

[30] The most significant environmental factor in EDL design and execution is the atmosphere of Mars, including both the magnitude and structure of density through the atmosphere and the velocity and frequency content of the winds during descent. The density structure of Mars impacts the peak acceleration and heating experienced by the Phoenix entry vehicle, as well as the altitude at which deployment of the parachute occurs (nominally ~13 km). The altitude of deployment in turn affects the time available to perform critical events prior to landing. A dynamic oscillatory mode called the "wrist mode," which is the swinging motion of the entry vehicle while suspended below the parachute, is sensitive to the frequency content of the wind at and below the parachute deployment altitude. The wrist mode dynamics can, in turn, affect the propagation of spacecraft attitude knowledge, radar ground acquisition, and attitude dynamics at separation events such as the separation of the lander from the backshell/parachute system (~1 km altitude). Wind velocity also has a significant impact on the spacecraft system velocity as it begins rocket-powered terminal descent (within the last 1 km altitude).

[31] Analysis of Phoenix EDL system performance through simulation is accomplished by both detailed analysis of simulated single trajectories, and statistical analysis via Monte Carlo methods with multiple simulated EDL trajectories with dispersed parameters. When executing Monte Carlo analysis, the EDL simulation tools simulate 2000 dispersed landings. Each simulated landing uses one of 2000 dispersed density profiles, and one of 2000 dispersed wind profiles. The statistical sensitivity of the EDL system to the ensemble of density and wind profiles is then assessed after finishing all 2000 simulations. This gives a measurement of EDL system performance across all expected landing conditions. With these techniques, the EDL system sensitivity to the atmosphere is assessed. EDL system design as well as selection of computer code parameters used during EDL is dependent on this process and thus dependent on how well both density and wind models represent the environment that will be encountered by the Phoenix spacecraft on landing day.

[32] Sections 2.5 and 2.6 below provide a description of the generation of the 2000 density and 2000 wind profiles provided to the engineering team, using the model output discussed above, and data, when available. Section 2.7 discusses some of the results of the Monte Carlo modeling efforts to date.

2.5. Wind Engineering Models

[33] Phoenix is slated to land in the late Martian afternoon in the northern lowlands. Few direct observations exist of winds at this time and location hence our estimates of wind conditions derive solely from the results of the modeling studies described in the previous sections. Understanding the effect of winds on risk assessment requires estimates of the wind variations on both large and small scales. Large-scale wind information is important for assessing hazards owing to shear and for targeting control, whereas vertical variations down to scales smaller than 25 m are deemed important for assessing the degree of excitation of the "wrist mode" during parachute descent.

[34] To model the effect of the large-scale mean wind, a "nominal" set of ~1800 vertical profiles of horizontal and vertical wind components was selected from a 20-sol run of the OSU MMM5 mesoscale model. The dust loading conditions for this run corresponded to the highest Conrath-nu value used in the mesoscale models and visible mean optical depth chosen of 0.075. The Conrath-nu parameter controls the distribution of dust in altitude as a function of latitude and was based on TES data [*Smith*, 2003]. This high Conrath-nu case was chosen because it produced strong winds suitable for rigorous risk assessment and was considered the most realistic dust distribution for this time of year and location. In general, simulations with greater dust loading tended to produce weaker wind regimes owing to diminution of the mean meridional temperature gradient across the polar cap boundary, though this is not the only controlling factor.

[35] For the selected landing location, the profiles were taken from the southern halves of landing site regions A and D, with the specific aim of capturing the potential effects of katabatic winds arising from the area near Alba Patera. The local time of each wind profile was constrained to lie within the range of 12 to 17.5 hours.

[36] An additional set of ~200 "outlier" profiles were added to the nominal set increasing the number used for Monte Carlo simulation to a total of 2000. The intended purpose was to produce a high-energy tail of the wind speed distribution providing some conservatism to the wind estimates, in part to compensate for the lack of observations and limited integration time of the mesoscale models. The outlier profiles, taken from an MRAMS model run, were collected as follows: The planet was divided into 72 regions, 5 degrees wide in longitude and extending in latitude from 30N to 90N. In each longitude bin, we selected the profiles that fell within the top 30% in terms of the total column-integrated kinetic energy they possessed below the 50-km level. The number of profiles contributed by all the bins far exceeded the desired number of ~200; consequently, profiles were chosen randomly from this superset to form the

final outlier set. Because the strongest winds are generally found where storms form near the polar cap edge, the outlier profiles come predominantly from a latitude band between 72N and 87N, although a small percentage come from clusters centered on −150 and −20 longitude in the latitude band from 30N to 40N.

[37] The vertical resolution of the mesoscale models is insufficient for resolving turbulent eddies at scales less than a few hundred meters, except near the surface. To simulate the presence of small-scale turbulence, a high-frequency, quasi-random wind field was superimposed on the large-scale nominal and outlier profiles described above, using a method similar to the turbulence addition (TA) process [*Kass et al.*, 2003, section 6.2] used for preparing MER engineering wind profiles (which was based on the Pathfinder wind modeling approach) [see *Kass et al.*, 2003, section 3.1; *Smith et al.*, 1995]. The primary modification was in the treatment of the vertical wind, but the significantly different sources of input TKE also resulted in quite different profiles. These are described further below.

[38] The TA process is a power spectral density (PSD) approach using a high-frequency component modeled on free air turbulence (−5/3 slope) with vertical frequencies windowed between 20 and 5000 m (in a Fourier series starting at 163 km). The amplitude and phases are generated randomly following the PSD curve. This process is used to generate a statistically constant-with-height high-frequency wind field for each direction, *u*, *v*, and *w*. The individual components are then scaled according to the vertical TKE profile to be "expanded." The TKE profile is supplied by the OSU LES model. Particularly for the "outlier" profiles, the TKE was also scaled up to get the desired degree of conservatism. The TKE is partitioned between the three directional components, with *u* and *v* each receiving 50%. On the basis of analyses of the LES model runs for Phoenix, the scaling of the *w* component is somewhat more complex. The partition for *w* starts at 30% near the surface increases parabolically to 60% at the midpoint of the turbulent layer and then decreases back to 30% at the top of the layer (defined as the altitude above the altitude of the peak TKE where the TKE value first drops to 10% of the peak value). Note that the energy in the three components is deliberately greater than 100%. This was done to make sure the resulting profile is sufficiently conservative for engineering purposes and also to more closely follow the MER approach. Also, owing to the random nature of the generation of the high-frequency component, individual profiles do not attempt to conserve energy. The profiles only conserve energy (modulo the 1.3 to 1.6 scaling factor in the component partitioning), in an ensemble mean sense.

[39] The use of turbulence profiles from the LES model had noticeably different results from those produced in the MRAMS mesoscale model, used in MER and previous iterations of the Phoenix wind engineering models. The convective boundary layer produced in the LES models extended to a depth of almost 8 km, with significantly higher TKE values. Furthermore, the LES models generated nonzero turbulence ($\sim$0.5 m^2/s^2) all the way to their model top at 25 km. The TA process used this energy to generate high-frequency structure (with the appropriate energy and maximum velocity) up to altitudes of 25 km. Some representative examples of wind profiles, including outlier profiles, produced by this process are shown in Figure 2.

[40] We also experimented with other techniques for adding small-scale winds to the mesoscale profiles before settling on the method described above. For example, in one method we added LES model wind components directly to the mesoscale profiles. This method had the appeal that the LES winds are derived from rigorous solution of the dynamical equations, including an appropriate solution for the late-afternoon thermal convection, whereas the TA approach described above is essentially phenomenological in nature. However, it was found to be computationally impractical to run the LES models with sufficient spatial resolution to resolve the mechanisms responsible for wrist-mode excitation; wind shears produced by the highest-resolution LES results were too small to excite the wrist mode as much as wind shears generated by the TA process. We also experimented with using the TA process in conjunction with TKE profiles taken from the MRAMS model rather than from the OSU LES model. This approach had the effect of confining the small-scale turbulence to a mixed layer near the surface below $\sim$5 km. In comparison, the LES model predicted a mixed layer extending up to at least $\sim$8 km, with substantial TKE penetrating to as high as $\sim$25 km in altitude. Because the TKE profiles derived from the LES model are based on a rigorous calculation of the mixed layer (whereas those from the MRAMS model are based on subgrid physical parameterizations) and because the small-scale winds derived using the LES model's TKE profiles provide a more stringent test of the spacecraft performance, we ultimately decided that the best course would be to use the phenomenological model in conjunction with the LES TKE profiles to generate small-scale winds for the EDL simulations.

2.6. Density Engineering Model

[41] Our approach to constructing trial density profiles for Phoenix EDL Monte Carlo studies largely follows that employed for the MER landings [*Golombek et al.*, 2003] and we give a brief overview below, but refer the reader to that paper for general background. However, there are several notable differences required for Phoenix. These differences include the suite of MGS TES data used; our approach to interpolating temperatures between the lowest TES level used and the surface; our approach to extending the TES temperature profiles, which on the dayside cluster around a local time of 1330 hours, to other local times within the landing window; and details associated with creation of perturbation temperature profiles designed to represent weather and climate phenomena.

[42] As discussed by *Golombek et al.* [2003], construction of the trial density profiles begins with creation of a mean or "baseline" temperature profile. The density models for Phoenix EDL are primarily based on TES temperature profiles retrieved from data acquired between 65° and 72° north latitude during Mars year 25 (November 2000) when L_s was in the range 73–83. We did not use data acquired during Mars year 26 because of a paucity of limb profiles available in the latitude range of interest. Temperatures at pressures higher than 0.25 mbar (i.e., below $\sim$34 km) were derived from nadir-sounded radiances and averaged over 5-degree latitude by 10-degree longitude bins. Individual

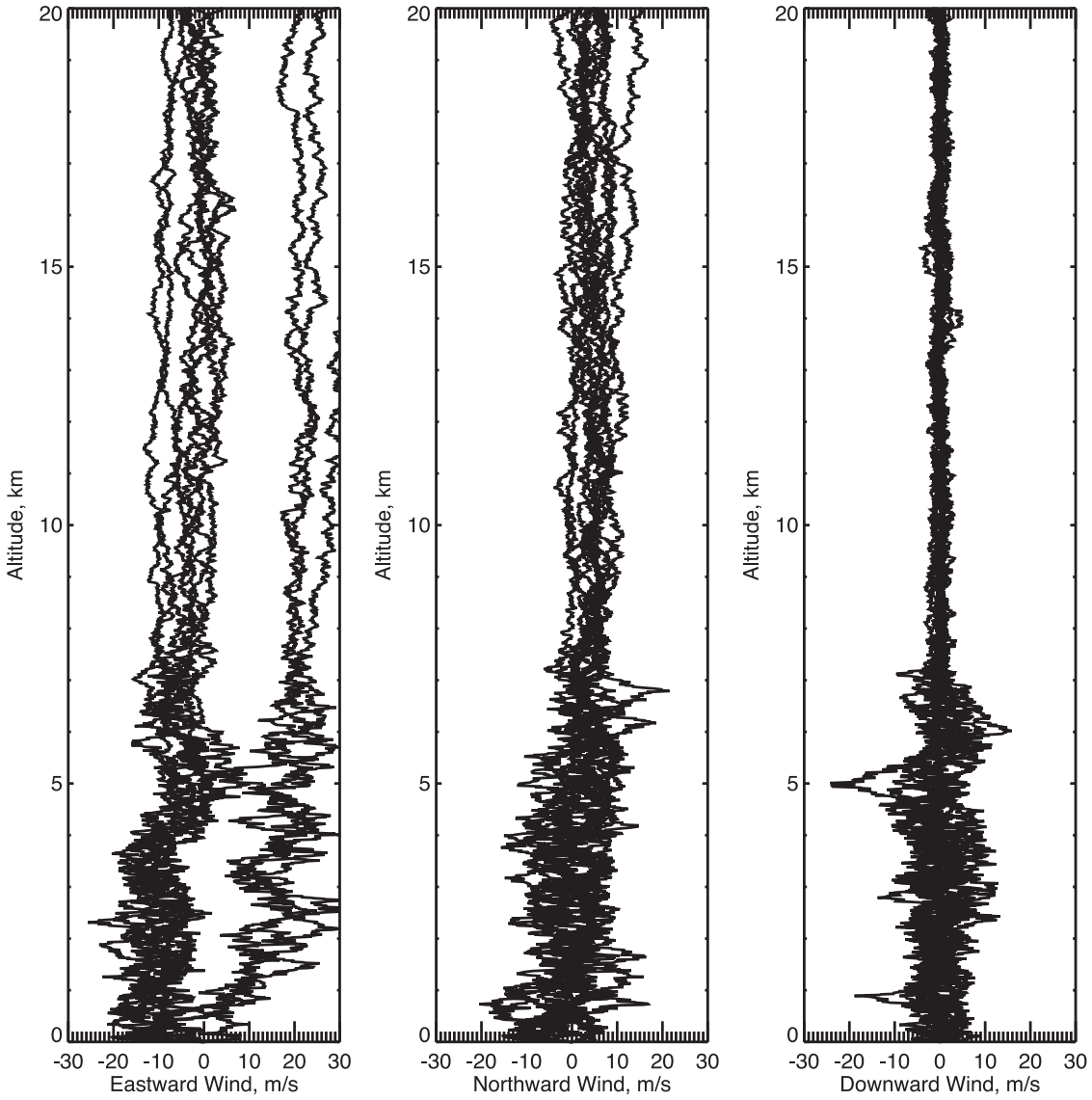

Figure 2. Altitude profiles created by the engineering model are shown for each wind component between 0 and 20 km, the altitude range for which the EDL process is most sensitive to wind. Ten representative profiles are shown in each panel. The high-frequency structure is contributed by the turbulence-addition model. A small sample of outlier wind profiles is included in this set and is most easily discerned from the positive eastward winds appearing in the first panel.

limb profiles supplied the temperature data at higher altitudes (lower pressures). The local time for all data used was restricted to fall within a 30-min-wide bin centered on 1330 hours. Temperatures were assumed to be isothermal at altitudes above the lowest pressure sounded (0.009 mbar ~60 km). We computed the zonal average of the binned nadir profiles to produce a low-altitude mean temperature profile. Similarly, the zonal average of the individual limb profiles was computed to produce a single high-altitude mean profile. The two profiles were then combined smoothly across the 0.25-mbar level to form a single temperature profile for altitudes between 2 and 130 km.

[43] The TES data were not used to construct the temperature profile at altitudes below 2 km, since their vertical resolution is insufficient for resolving the superadiabatic temperature gradient near the surface. To extend the model temperature profile to the surface, we rely on the zonal average of MRAMS mesoscale model profiles. These profiles were restricted to the same set of latitudes and local times as the TES data. The low-altitude profile was joined across the 2-km level to the mean TES profile using a parabolic interpolation involving the four altitude grid points closest to the 2-km level. We refer to this combined profile as our "baseline profile" for 1330 LT.

[44] The daytime TES data are restricted to between 1300 and 1400 LT. Since the local time at Phoenix arrival is 1620 LT (and prior to the launch date being known it varied even more), it was necessary to extend the baseline profile for 1330 LT to other local times. We accomplished this by calculating the zonal-mean temperature tendency produced by the MRAMS model as a function of latitude, altitude, and local time. Baseline profiles at other local times were

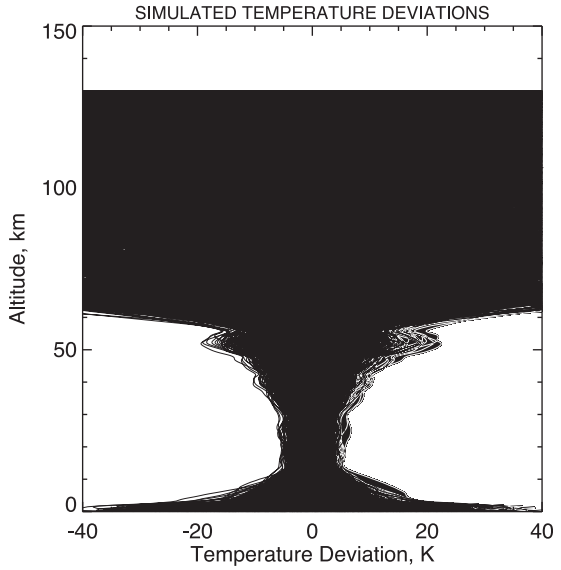

Figure 3. Temperature deviations for the nominal model. Two thousand trial profiles are shown.

then constructed by integrating the 1330-hour baseline profile forward and backward in time using the temperature tendency model data to give the time rate of change of the zonal mean temperature. This integration was applied to the entire baseline profile between 0 and 130 km.

[45] To represent the effects of weather, climate, and waves on temperatures, it is necessary to add a vertically varying perturbation to the baseline profile. Our approach for Phoenix essentially follows that of *Golombek et al.* [2003], but there are notable differences. Using temperature variances produced by the MRAMS model to gauge the expected level of temperature variability at each altitude level, vertical profiles of perturbation temperature were constructed as follows. We selected a set of 2000 MRAMS temperature profiles falling within the latitude and local time range of interest and calculated their deviation from the mean over the set at each altitude level. The maximum of the absolute deviation over this set of profiles was then compiled as a function of altitude, and each vertical profile of temperature deviation was then normalized by this envelope function, A(z). Each of the 2000 normalized profiles was then fit as a function of altitude by a Chebyshev polynomial of order 400. This produces 400 distributions of 2000 coefficients for each order in the polynomial. The variance of each distribution was calculated, and the associated standard deviations were scaled upward by a factor between 3 and 4 to ensure a conservative estimate would be made of the degree of temperature variability that might be encountered during EDL. This enhanced standard deviation was then used to characterize a normal distribution for the coefficients corresponding to each order of the polynomial. Two thousand random Chebyshev coefficients were then generated for each order, and after multiplication by A(z), a new set of 2000 random temperature deviation profiles were created from the new polynomials. These were then added to the baseline profile to create our set of 2000 trial temperature profiles.

[46] The MRAMS model was also used to estimate the variability of surface pressures in the latitude and local time range of interest. The typical standard deviation of surface pressure was found to be $\sim$0.1 mbar. We increased this standard deviation by as much as a factor of 3 to account for the uncertainty in actual conditions that may be encountered. A random set of 2000 surface pressures was generated using a normal distribution characterized by the enhanced standard deviation.

[47] Given a trial surface pressure and temperature profile, the dependence of pressure on altitude is determined by the hydrostatic equation, and the trial density profile is then determined using the ideal gas law. A "tornado plot" of the trial temperature profiles used for a nominal clear atmosphere is shown in Figure 3. The standard deviation of the temperatures near the base of the model is $\sim$13 K. The associated density variations are shown in Figure 4, where the variations are expressed in terms of the fractional deviation from the baseline density profile. Fractional density variations in this model can reach 25% near the surface and much higher values above 50 km.

[48] The Martian atmosphere is usually relatively free of dust at the latitudes and season of the Phoenix landing. However, the possibility of encountering atypically dusty conditions has led us to construct a baseline profile representative of a relatively dusty atmosphere. The process of adding temperature perturbations to this dusty baseline profile was the same as that described above for the nominal baseline. To construct a dusty baseline profile, we followed the approach developed by one of us (D. Kass) for the MER mission. Briefly stated, high-latitude TES temperature profiles for L_s = 215 were collected for Mars years 24 and 25. The atmosphere during Mars year 24 (1999) was relatively dust-free at L_s = 215 whereas it was considerably more dusty during Mars year 25 owing to the presence of the global dust storm of that year ($\tau_{vis} \sim 5$). Both nadir and limb profiles were used and combined in the same manner as for the nominal case. Extension of the TES profiles to the surface was achieved using MRAMS results for an atmosphere with globally uniform visible optical depth of 0.5.

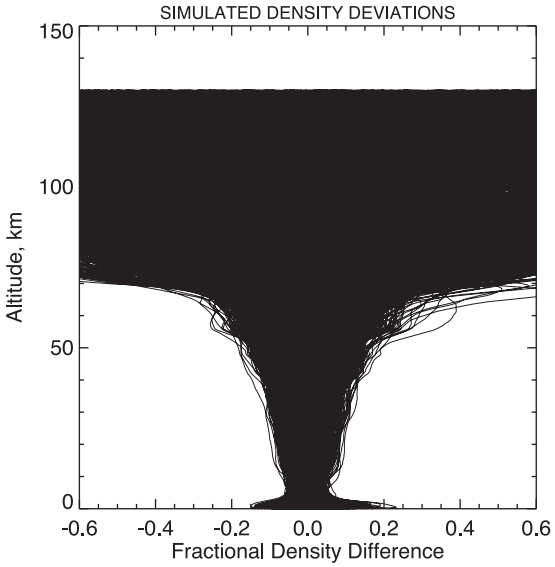

Figure 4. Fractional density deviations relative to nominal baseline profile, corresponding to the temperature variations shown in Figure 3.

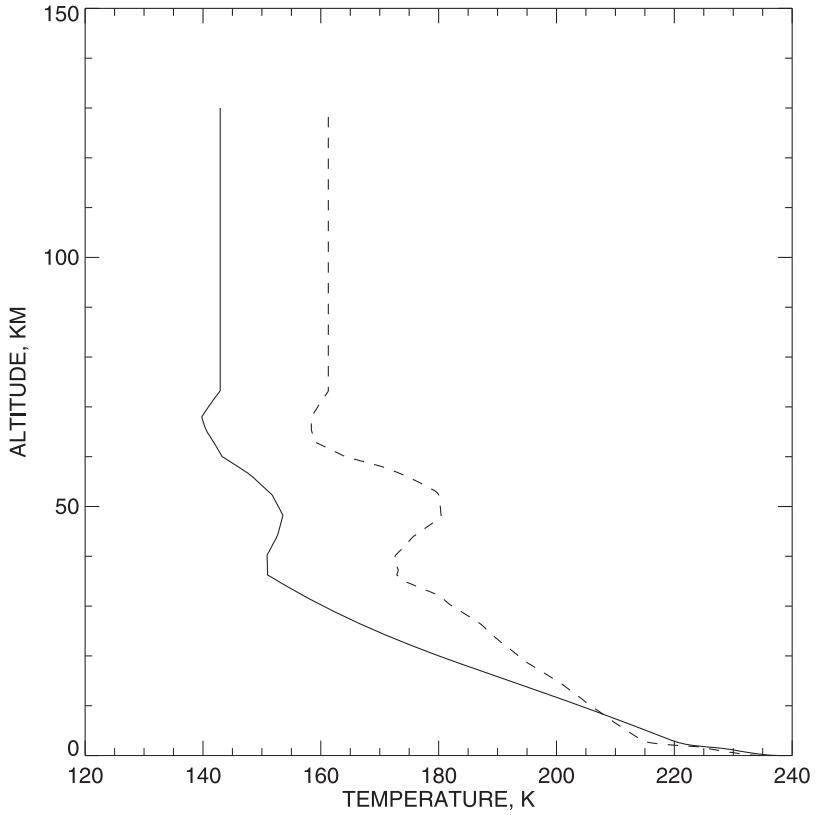

Figure 5. The atmospheric temperature profiles for the dusty baseline profile (dotted) compared to the nominal baseline profile (solid).

The means of the temperature profiles for the two years were found, and the difference $T_{dust} - T_{clear}$ between the "dusty" profile and clear profile was calculated to define a "dust effect." The difference was then added to the nominal baseline profile corresponding to $L_s = 73-83$ to create the dusty baseline profile. This dusty baseline profile is shown together with the nominal one in Figure 5. The thermal perturbations from a global dust storm, used here, are larger and extend over a greater atmospheric depth than for a local storm that would be more typical for the Phoenix landing location and season. This will lead to larger density deviations than for a local storm and were seen to exceed the differences seen in the various mesoscale runs we conducted.

[49] As mentioned previously, both the nominal set of density profiles and the dusty set are used in Monte Carlo analyses to design the EDL system and select appropriate computer program parameters. These profile sets help ensure that the Phoenix spacecraft will land successfully to a high degree of confidence. Some results are presented below.

2.7. EDL Results

[50] The current results of Monte Carlo analyses of the Phoenix Lander system using the above density and wind profile sets indicate that the Phoenix EDL system is comfortably inside the desired range of performance levels. The key EDL system metrics affected by different density and wind profiles are summarized in Tables 1–3. In particular, Table 1 shows the metrics affected by density profiles and the performance of the spacecraft when using the 2000 density profiles in a Monte Carlo model. On the basis of the Monte Carlo results, the mean value of each metric is shown. The 99% high (low) value for each metric represent the data point for which 99% of the runs produced lower (higher) values. As the desired range column indicates, the Phoenix EDL system is comfortably inside the desired range of performance levels, and is robust to the level of the density dispersion modeled in the atmosphere models provided by the Phoenix atmosphere modeling team.

[51] Tables 2 and 3 summarize the key EDL metrics sensitive to winds: wrist mode behavior and velocities at

Table 1. EDL Performance Metrics Sensitivity to Density

EDL Metric (Mean Altitude of Event)	99% Low	Mean	99% High	Desired Range
Peak deceleration (34.3 km)	8.5 g	9.2 g	9.9 g	<13 g
Peak heating (41.5 km)	44.2 W/cm^2	45.9 W/cm^2	47.5 W/cm^2	<64 W/cm^2
Total heating (N/A)	2267 J/cm^2	2367 J/cm^2	2471 J/cm^2	<3320 J/cm^2
Altitude at parachute deploy (16.3 km)	9.7 km	12.8 km	16.3 km	N/A
Mach at parachute deploy (16.3 km)	1.44	1.67	1.97	1.3–2.13
Dynamic pressure at parachute deploy (16.3 km)	455 Pa	492 Pa	536 Pa	300–540 Pa

Table 2. EDL Wrist Mode Rates Affected by Wind Frequency Content

EDL Metric (Mean Altitude of Event)	99% Low	Mean	99% High	Desired Range
Wrist mode rate at heat shield separation (11.1 km)	1.4 deg/s	16.4 deg/s	54.4 deg/s	<100 deg/s
Wrist mode rate at lander leg deploy (10.4 km)	1.3 deg/s	15.2 deg/s	52.0 deg/s	<100 deg/s
Wrist mode rate at radar on (6.9 km)	1.5 deg/s	17.2 deg/s	53.9 deg/s	<100 deg/s
Wrist mode rate at radar ground lock (2.1 km)	3.1 deg/s	30.8 deg/s	83.6 deg/s	<100 deg/s
Wrist mode rate at lander separation (0.9 km)	3.5 deg/s	35.4 deg/s	97.1 deg/s	<100 deg/s

lander separation from the backshell. As Table 2 illustrates, the lander wrist mode rate remains below the desired level, <100 degrees/s, for most of the metrics, but is approaching the limit of the desired range near lander separation. This increase in rate at lower altitudes occurs as the EDL system enters the more turbulent mixed layer below ~8 km, and is an example of the value of the wind profiles in providing key insights into EDL system behavior. Table 3 summarizes the vertical and horizontal velocities at lander separation, a key EDL system sensitivity to steady state winds. The velocity of the vehicle at lander separation must be reduced to near zero before touchdown, and thus excessive velocity at lander separation challenges the Phoenix propulsion system and increases fuel use. The statistics in Table 3 show that winds modeled in the Phoenix EDL simulation result in velocities at lander separation that are within the desired range.

2.8. Atmospheric Update Process

[52] About two months prior to landing, we will begin to monitor the atmosphere at the Phoenix landing latitudes regularly. We plan to make use of the Mars Reconnaissance Orbiter (MRO) Mars Color Imager (MARCI; *Malin et al.* [2001, 2007]) and Mars Climate Sounder (MCS) experiments. The MCS is an atmospheric profiling instrument [*McCleese et al.*, 2007] that will enable us to monitor the atmospheric temperatures as a function of height from the surface to 80-km altitude with approximately 5-km resolution. These profiles will be used as a comparison to the profiles generated, using TES data, in our engineering density models described above. In this way, we will be able to tell if the atmosphere is substantially different than what has already been provided to the engineering team or not, and whether regeneration of a new set of 2000 density profiles is warranted. In the last several weeks prior to landing, we will evaluate the MCS profiles on a daily basis. The MARCI camera will enable us to see any dust storm that could affect the landing location on landing day and will provide context for interpreting the MCS profiles.

3. Surface Operations

3.1. Overview

[53] Phoenix spacecraft health and safety and operational capabilities during the surface mission also depend on an understanding of characteristics of the local environment. Diurnal surface and near-surface atmospheric temperatures and near-surface winds are needed for thermal control of the spacecraft. These thermal model inputs are often provided by atmospheric modeling that makes use of typical surface characteristics such as albedo and thermal inertia of the potential landing site. Dust and water-ice optical depth minimum, maximum and variability are needed to verify the solar panel and battery capabilities and to estimate the amount of power and energy needed to operate the spacecraft and collect science observations throughout the mission. Dust storm statistics are needed to verify that the spacecraft power system will withstand a certain level of storm length and optical depth and to ensure that the mission will last its mission lifetime. Most of these quantities are obtained through analysis of the current data sets for a given location and season on the surface of Mars.

[54] Because there are both engineering and science needs for modeling and data analysis of the atmospheric characteristics of Phoenix mission's landing location and season, a lot of work has gone into understanding them over the last several years. Below, we describe some of the atmospheric characteristics expected during the Phoenix mission.

3.2. Surface Pressure

[55] Surface pressure data from landing through the nominal mission length (90 sols on Mars), was also needed for spacecraft thermal predictions as it is one of the parameters used in an empirical relationship to estimate surface convection heat transfer coefficients; temperature, wind speed, and characteristic dimension are the other three parameters used. The surface pressure range for the high northern latitude Phoenix landing zone (65–72N) is estimated to be between 7 and 11 mbar. While Phoenix has recently (March 2007) downselected to a 150 × 40 km box centered near 68N, 233E, analysis was needed for the entire longitudinal annulus, to allow for a variety of landing sites to be considered. The pressure range provided was scaled from Viking Lander 1 and 2 (VL1 and VL2) data via the Ames Mars Global Circulation Model (GCM; *Haberle et al.* [1999]) to the Phoenix landed elevation range and includes a 10% margin for dynamical effects and additional uncertainty. The surface pressures are highly correlated with topographic height. Within the Phoenix landing latitude band, the highest elevation is −3500 m with respect to the MOLA datum and the lowest elevation is −5419 m [see also *Arvidson et al.*, 2008].

[56] To determine the proper range of values, the Ames Mars GCM was first checked against VL1 and VL2 pressure data, as these observations are our best long-term data. The GCM point nearest the Viking Lander sites [VL1 (22.48N, 47.730W); VL2 (47.669N, 134.206E)] was obtained. The topography in the nearest Ames GCM points was −3874 m for VL1 and −4262 m for VL2. For comparison, the MOLA

Table 3. EDL Lander Separation Velocities Affected by Steady State Winds

EDL Metric (Mean Altitude of Event)	99% Low	Mean	99% High	Desired Range
Vertical velocity at lander separation (0.9 km)	45.6 m/s	54.3 m/s	63.2 m/s	<65 m/s
Horizontal velocity at lander separation (0.9 km)	3.4 m/s	10.8 m/s	25.1 m/s	<30 m/s

elevations of the landing sites for VL1 and VL2 are −3620 m and −4507 m, respectively. Thus, the GCM point was too low at VL1 and too high at VL2 and therefore an altitude correction had to be performed using the hydrostatic equation. The GCM result was almost uniformly too low by ∼0.1 mbar at VL1and too high at VL2 by ∼0.3 mbar. Thus, the GCM is able to determine the pressure to within ±0.3 mbar, and with added margin the GCM is estimated to be accurate for any location to within ±0.4 mbar.

[57] To determine the range of values for the Phoenix landing annulus, several GCM points at 70°N (corresponding to regions A, B, and C) were selected. The highest elevation in the allowable Phoenix landing zone is −3500 m and the lowest is −5419 m [*Arvidson et al.*, 2008]. Pressures from the GCM at 70°N were hydrostatically adjusted to these elevations and the margin of ±0.4 mbar was added, yielding a pressure range of 7.8–10.0 mbar. Surface pressure for a GCM point near −3500 m and within the landing latitude annulus of 65°–72°N was checked against this estimate and good agreement was found.

[58] Finally, the margin simply takes into account the offset between the model and the Viking Landers. There may be other errors and also dynamical effects will likely add an additional 5% uncertainty. As such, a 10% uncertainty was added, yielding the range of 7.0–11.0 mbar.

3.3. Visible Optical Depth

[59] The visible optical depth was needed by the Phoenix team to model the thermal environment on the spacecraft and the available energy for the duration of the surface mission operations (90 sols; $L_s \sim 76–117$). Both dust and water-ice optical depth will contribute to the resulting spacecraft temperatures and energy availability. Dust optical depth varies much more than that for water ice so we defined the total visual optical depth as a function of season for the "nominal" or typical dust loading conditions and that for a dust storm case. For engineering purposes, we defined the "required" optical depth that was used for energy and thermal modeling by the spacecraft team. The data and methods used to determine the optical depth values are described below.

3.3.1. Nominal Conditions During Surface Operations

[60] We collected water-ice and dust optical depths for three Mars years (MY 24–26; after *Clancy et al.* [2000]) of MGS TES data over all longitudes between 65° and 72°N and for the entire landed mission duration of 90 sols. Including data at all longitudes and over multiple years ensured that temporal and spatial variability was captured to the best extent possible. Since the TES quantities as provided are absorption-only infrared optical depths, we converted them to full extinction, visible optical depths and then combined water ice and dust for a total atmospheric optical depth.

[61] The dust conversion is described here. Both *Smith* [2004] and *Wolff and Clancy* [2003] suggested a multiplicative factor of 1.3 to convert from absorption-only to full extinction optical depths. To convert from infrared (∼9 micron) to visible (∼0.7 micron), the particle size is important. If one assumes particle sizes of 1.5 (effective variance of 0.4) a multiplicative factor of 1.7 is suggested [*Clancy et al.*, 2003]. Thus, the total multiplicative factor used for dust was 2.2 or $\tau_{dust,IR,abs} \times 1.3 \times 1.7 = \tau_{dust,vis,ext}$.

[62] To convert water-ice absorption-only optical depths to full extinction, a multiplicative factor of 1.4 is suggested by *Wolff and Clancy* [2003] and 1.5 by *Smith* [2004] (for absorption-only optical depths <0.5, appropriate for most of the water-ice optical depth retrievals in the polar region). To convert water-ice optical depths from infrared (∼12 micron) to visible (∼0.7 micron), again particle size is important. *Clancy et al.* [2003] see particle size variations with season and location, with their type 1 clouds seen in the polar region. This type has a smaller particle size (radius of 1–2 μm and effective variance of 0.1) and suggests a multiplicative factor of 3.0 for the IR-to-vis conversion (M. Wolff, personal communication, 2004; see also *Wolff and Clancy* [2003]). Thus, the total multiplicative factor used for water-ice was 4.2 or $\tau_{ice,IR,abs} \times 1.4 \times 3.0 = \tau_{ice,vis,ext}$.

[63] With the TES optical depths converted to full extinction, visible quantities and combined for total optical depths, we zonally averaged the data for all 3 Mars years and within the landing latitude annulus for every 0.5° L_s throughout the planned landed mission (Figure 6). The means for each seasonal bin were then plotted and a third-order polynomial was fit to the curve such that the resulting equation could be used by the engineering team to predict the optical depth for any given seasonal date. The curve created by the mean values was used by the engineering team as a nominal or expected case. The standard deviation of the means, representing the variability in the data, was also calculated, added to the means, and fit with a third-order polynomial. This curve was used by the engineering team as a "worst case" for planning purposes. As shown in Figure 6, the nominal range throughout the mission is a total optical depth of about 0.3–0.6 and the worst-case range varies between about 0.4–0.9, with larger optical depths earlier in the season. If the mission continues past the 90th sol ($L_s \sim 117°$), then in general the optical depths tend to increase again as the season progresses into northern fall.

3.3.2. Dust Storms

[64] In order for the engineering team to understand how well the solar-powered Phoenix Lander will perform (power and thermal) under heavy dust loading conditions, a dust storm "requirement" was developed through analysis of the MGS Mars Orbiter Camera (MOC; *Malin et al.* [1992]) and TES data. The most useful information for the engineering team was a "worst-case" dust storm optical depth magnitude and duration. We defined this to be a dust storm having a visible optical depth of 2.5 for 3 sols.

[65] Analysis of MOC images shows that dust storm activity between 65° and 72°N, the Phoenix landing latitude zone, during the late northern spring through midsummer seasons was isolated to transient local events (i.e., covering an areal extent less than 1.6×10^6 km^2 with dust-lifting activity persisting for less than 3 sols). About 80% of the storms persisted over a given location for ∼1 sol, even those associated with traveling cold fronts. Figure 7 shows storm activity across the four longitude quadrants (0–90°W, 90–180°W, 180–270°W, 270–360°W) was relatively infrequent during the 4 Mars years spanning from November 2000 through October 2006. Peak activity appears for the most part to have occurred between $L_s \sim 70$ and 85° (the Phoenix landing season), with the exception of a midsummer, L_s = 130–145°, peak between 0 and 90°W. Larger regional

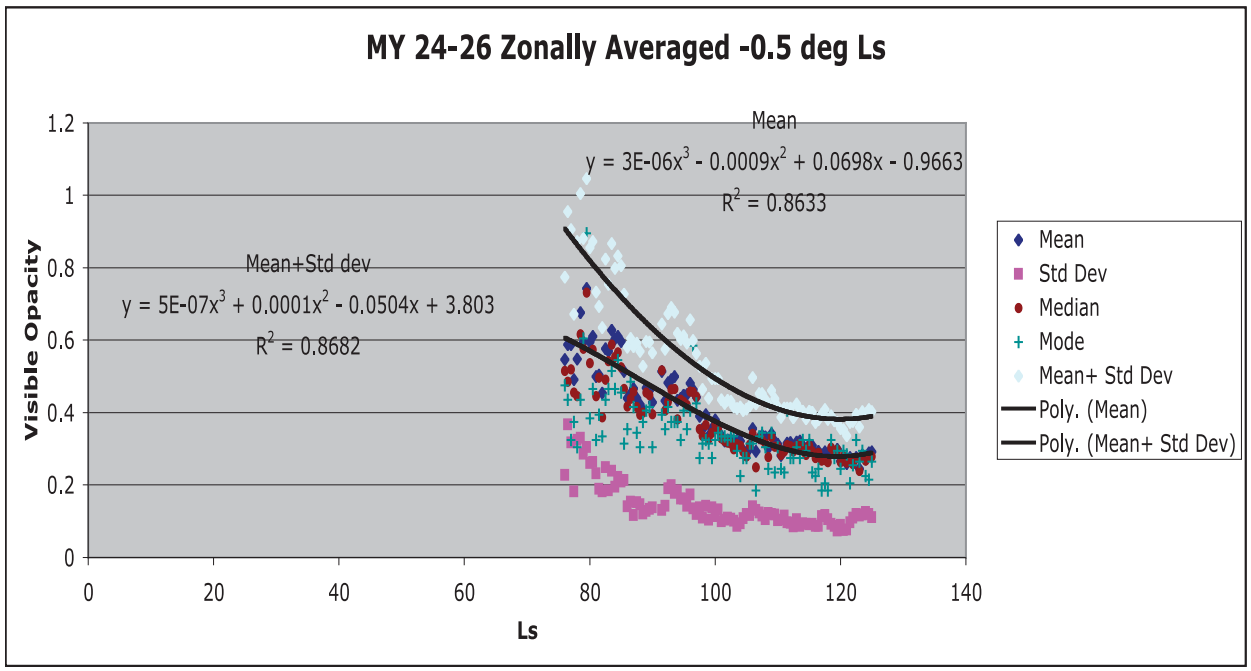

Figure 6. Visible opacity means and standard deviations for three Mars years of TES dust and water-ice opacity data averaged over latitudes of 65–72°N and by 0.5 L_s (~1 sol). A third-order polynomial was fit to the mean values and to the mean plus standard deviation values.

storms were not observed until after the primary mission (L_s > 130°).

[66] Observations of dust storm activity by TES in the latitude band 65°–72°N during the period of the Phoenix nominal mission (L_s = 73°–117°) and beyond, were also examined for dust storm occurrence and magnitude. These data show no regional or global-scale dust storms, but intense local-scale dust storms with visible optical depth greater than unity are not uncommon [*Smith*, 2004, 2006]. Individual local-scale dust storms cannot be tracked using TES data because ground tracks do not repeat on a daily basis, but it is evident from the stochastic appearance of these dust storms in the data that they do not last longer than a few sols before dispersing. Images from MOC [*Cantor et al.*, 2001], which can track the daily movement of small dust storms, confirm that local-scale dust storms at this latitude and season do not persist longer than 3 sols, as stated above. Further information on the duration of local-scale dust storms at equatorial latitudes has been obtained by observations made by the Mars Exploration Rovers [*Smith et al.*, 2006; *Lemmon et al.*, 2004], which show that local-scale dust storms last no longer than about 3 sols as dust can clear quickly by wind blowing the dust cloud to an adjacent location. Thus, on the basis of both MOC and TES data, a dust storm worst-case duration of 3 sols was provided as a requirement to the engineering team.

[67] The value provided as the worst-case dust storm optical depth magnitude was estimated two ways. First, we examined a cumulative frequency plot covering two Mars years (25 and 26) of TES data for the Phoenix landing latitude zone and season (Figure 8). This figure shows that dust optical depths (full-extinction, visible) reach nearly 2.0. Second, we examined MOC images of dust storms in the polar region during summer and confirmed that dust storms exist with optical depths greater than unity, consistent with TES. However, because only two complete Phoenix landed seasons were available in the TES data, and these data may not fully represent the variability of dust storms at this latitude and season, a "requirement" of dust optical depth equal to 2.5 was provided to the engineering team.

3.4. Wind Estimates

[68] Winds during the surface mission are important in terms of their thermal effect on the spacecraft. Interestingly, the engineering team desires some wind during the peak

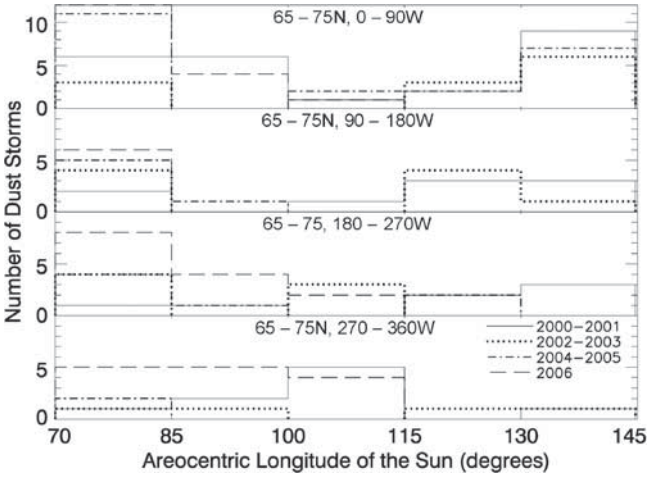

Figure 7. The frequency of dust storm activity observed at Phoenix latitudes in MOC wide-angle observations as a function of L_s, using a bin size of 15° of L_s. MOC observations span the late northern spring and midsummer seasons over four consecutive Mars years from November 2000 to October 2006. No distinction between local and regional storms was made.

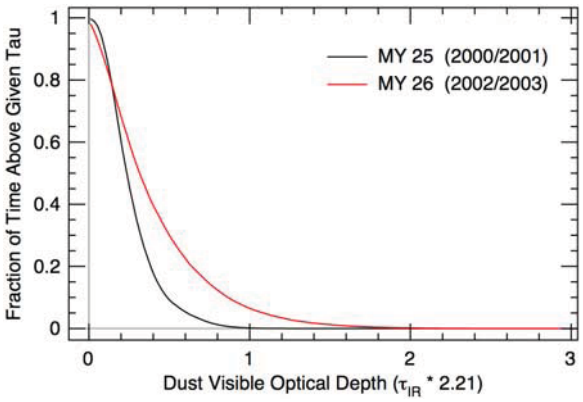

Figure 8. Full extinction, visible dust optical depth cumulative frequency plot for TES observations in the Phoenix latitude annulus and over the Phoenix landed season for Mars years 25 and 26.

daytime temperatures, to ensure the spacecraft will stay cool. On the other hand, at night, they desire low winds so that the spacecraft will not get too cold and require too much energy for heater operation. Additionally, gusts could perhaps clean off solar panels, as happened during the MER mission [e.g., *Stella et al.*, 2005], raising the total power generation back to earlier mission levels. For design purposes, the engineering team is concerned mostly with sustained winds, not very short (order of minutes) gusts. As such, we defined the minimum and maximum sustained wind over an entire diurnal cycle as well as maximum sustained winds over a few minutes to a 4-hour block of time.

[69] Near-surface wind estimates for the Phoenix landing latitude and season are obtained from OSU and SwRI mesoscale model output, as no actual data currently exist for this region. The OSU and SwRI model output characteristics are described in Table 4. Winds from each model were examined for regions A, B, and C and averaged in 2-hour bins. Figure 9 shows region A (next to region D) output for each model. The grid points are on the order of tens of kilometers spacing, so very local wind effects are not resolved. The 2-hour averaged wind speeds show values as high 10 m/s, but the models may only be accurate within a factor of 2, so conservatism was added yielding an engineering requirement of 20 m/s average continuous winds over a 4-hour period. For continuous diurnal winds, a wind speed of 15 m/s was recommended for the maximum, continuous (e.g., 24.7-hour) wind speed. Further, gusts of a few minutes or so can be up to 30 m/s (saltation speeds), as evidenced by observed dust uplift during storm fronts. As some of the 2-hour averages in Figure 9 show $\leq$1 m/s, a continuous, diurnal sustained low wind speed was estimated to be 0.5 m/s. As a further check, we examined average wind speeds at the VL2 site ($\sim$48 N) and they are consistent with the model output used here.

[70] The model output shows that the diurnal variation between regions is not consistent and predictable. This is likely due to the fact that the winds are primarily controlled by storm systems that can be passing over a particular location at any time of the day. As such, any diurnal variability shown in the examples (Figure 9) should not be assumed to be real; any wind speed shown could be observed at any time of day.

[71] In summary, MRAMS and OSU mesoscale and LES results indicate that the mean near-surface winds within the Phoenix latitude band should be less than 15 m s^{-1}. However, during the period each day where convective turbulence is prevalent, the landed spacecraft will experience significant perturbations about the mean wind magnitude. At other times of day, when convective turbulence is at a minimum, the MRAMS results indicate that the landed spacecraft may experience prolonged periods of winds less than 2 m s^{-1}. During the passage of a baroclinic storm system over the landed spacecraft, it appears likely that winds at all times of day will generally increase compared to nonstorm conditions.

3.5. Surface and Near-Surface Atmospheric Temperature

[72] The surface and near-surface atmospheric temperatures are also important for spacecraft thermal design and/or optimization and power usage estimates. Using expected and bounding albedo, thermal inertia, optical depth, and surface pressure, we ran the 1-D radiative-convective model from the Ames GCM [*Haberle et al.*, 1999; *Martin et al.*, 2003] to predict bounding temperature cases (65 N for daytime and 72 N for nighttime) during the Phoenix mission season (L_s = 76°–117°). This model has also been used in a similar fashion for the Mars Pathfinder, Mars Exploration Rover, and Mars Science Laboratory missions.

[73] The selection of input parameters to the 1-D model was driven by the needs of the engineering team. To test and optimize for the range of conditions that may be experienced by the lander, they required several cases: maximum daytime temperature and minimum nighttime temperature expected during the mission lifetime, minimum daytime temperature expected during a dust storm, and landing day (sol 0) min, max, and nominal temperatures. These cases are shown in Table 5 and are described below.

[74] Initial GCM simulations indicated that the surface thermal environment was not particularly sensitive to landing site pressure, so an intermediate value of 8.4 mbar was chosen. The values chosen for visible optical depth were selected on the basis of analysis of the same set of MGS TES data discussed above [see also *Tsuyuki et al.* [2007]). Albedo and thermal inertia values were chosen to drive the temperatures appropriately up or down and were selected to be consistent with the values observed in the Phoenix landing regions [*Putzig et al.*, 2005]. The latitude and L_s

Table 4. Characteristics of the OSU and SwRI Mesoscale Model Output Used to Estimate Near-Surface Wind Speeds During the Mission

	Height Above Ground Level (m)	L_s	Visible Dust Optical Depth	Number of Sols	Grid Spacing (km)
OSU	1.7	80, 120	0.05, 0.1, 0.075	20	18
SwRI	15	80	0.05, 0.3, 0.5	10	16.67

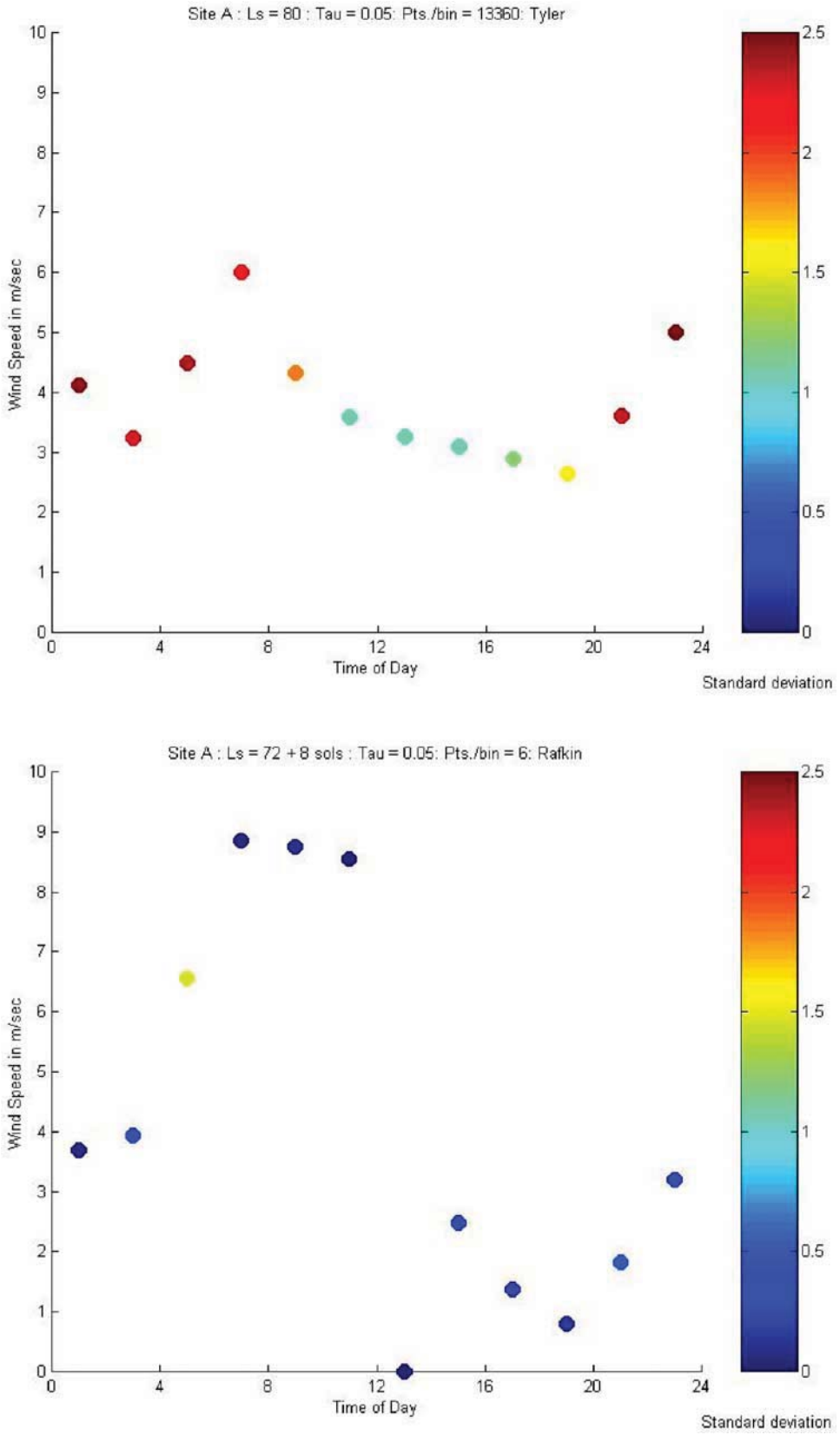

Figure 9. Region A mesoscale model output from the OSU model for (top) L_s = 80, visible dust opacity = 0.05, and from the SwRI model for (bottom) L_s = 75.77 (L_s = 72 + 8 sols), visible dust opacity = 0.05. The placement of the dot is the mean winds for the 2 hours centered on that point and the color bar gives the standard deviation. For the OSU model, each point plotted is an average of 13,360 points, and for the SwRI model, each point plotted is an average of 6 points.

Table 5. Ames One-Dimensional Model Input Parameters for the Various Surface and Near-Surface Atmosphere Temperature Predictions

Case Description	Optical Depth (τ)	Surface Albedo (A)	L_s	Pressure (mbar)	Thermal Inertia (J m^{-2} K^{-1} s$^{-1/2}$)	Latitude (°N)
Maximum daytime	0.12	0.1	110	8.4	210	65
Minimum nighttime	0.08	0.25	125	8.4	150	72
Minimum daytime: dust storm	2.5	0.23	125	8.4	300	72
Sol 0 maximum daytime	0.20	0.1	76	8.4	210	65
Sol 0 minimum nighttime	0.20	0.25	76	8.4	150	65
Sol 0 nominal	0.39	0.23	78	8.4	250	70

were also selected to be driving conditions within the landing latitude zone and primary mission season. The selected GCM input parameters are shown in Table 5 and a more complete description of the selection process is given by *Tsuyuki et al.* [2007].

[75] The first two cases, maximum daytime temperature and minimum nighttime temperature expected during the mission provided the overall bounding temperatures for the spacecraft to withstand. Since Phoenix will be operating during northern summer within the Mars arctic circle, the sun will be above the horizon at all times of day. We have defined ''daytime'' for operational and analysis purposes to be between 0900 local solar time (LST) and 1600 LST. ''Nighttime'' comprises the rest of the diurnal cycle. The maximum daytime temperature that the lander will experience will be increased by the operation of instruments, since ''daytime'' is when most science operations will be done. During ''nighttime'' the Phoenix Lander will be placed into a ''sleep'' operational mode (i.e., low electrical power demand and low self-heat generation) and will rely primarily on batteries. Periodic short awakenings will be performed to maintain the health of the spacecraft. Demand for ''keep-alive'' heater power will be based on the nighttime temperature expected. In addition, the driving latitude was chosen for each case. The maximum daytime and minimum nighttime temperatures both result when the optical depth is a credible minimum owing to maximum solar insolation and maximum thermal radiation from the ground, respectively.

[76] As discussed above, Mars is known for local and regional dust storms where the optical depth can be much greater than 1.0. Because a dust storm will reduce insolation on and therefore the power generated by the solar arrays, the flight system will resort to a minimum operational state, if needed, to endure the storm. For purposes of analysis, a minimum daytime temperature under a dust storm condition of $\tau_{vis} = 2.5$ provided the worst condition for power system assessment. A minimum nighttime temperature during a dust storm case was not a driver, as nighttime temperatures increase with opacity.

[77] Landing day, sol 0, presents a unique challenge to Phoenix. With all the pyrotechnic events during EDL, the batteries will be at a relatively low state-of-charge upon landing. The ability of the spacecraft to survive the first Martian night was a critical condition. Sol 0 was divided into a bounding hot and cold condition as well as an expected one and analysis was performed for each case.

[78] Table 6 summarizes the results for the various cases and TES ground temperatures are also provided for comparison. The GCM minimum diurnal ground temperatures for the maximum daytime and minimum nighttime cases were within 5°C of TES measurements. However, the maximum diurnal ground temperature comparison was different by as much as 20°C, with the 1-D model results being warmer than the TES data. The TES data have been averaged over the entire landing latitude annulus whereas the 1-D model was targeted to a specific areal ''domain'' which may not have the exact combination of surface characteristics as the zonal mean Martian surface. The thermal estimates provided for spacecraft analysis were considered conservative, yet credible. Given the Phoenix landing latitudes and the relevant input parameters, the ground temperature range is expected to be between 185.2 and 271.0 K. Likewise, the near-surface air temperature is expected to be between 189.1 and 256.7 K.

4. Discussion and Summary

[79] As discussed throughout this paper, understanding the atmospheric density profiles, via temperatures and pressure, and the range of behavior of the winds during spacecraft entry, descent, and landing (EDL) are critical to landing safely on Mars. We are fortunate to have had two orbiting spacecraft, MGS and MRO, each with instruments capable of measuring the atmospheric temperature profiles at the Phoenix landing location and season, providing both the historical record for the past few Martian years (MGS) and proving the latest atmospheric sounding just prior to entry (MRO). These data sets greatly help lower the risk associated with EDL. The same is not true for atmospheric winds however. In the case of winds, we must rely exclusively on model output, as no data are currently available near the Phoenix landing location. As such, future wind measurements on Mars should be considered a priority in the Mars program, since they are valuable not only scientifically, but also for future spacecraft landing safety and for thermal design of landed assets.

[80] The wealth of Mars spacecraft and their data in the past decade have also greatly enabled a better understanding of the surface albedo and thermal inertia, surface temperatures, and dust and water-ice cloud optical depth variability with time and location. These data are necessary for the proper design of and operational planning for a surface mission. Continuing a robust Mars program with ongoing orbital observations of the surface and atmosphere will further enhance our understanding of the climate and weather on Mars.

[81] As discussed in this paper, we expect the Phoenix landing location to likely experience winds, temperatures, pressures, and optical depths that are modest and we have optimized the spacecraft systems and entry, descent, and landing events to handle the expected conditions with margin. In particular, the expected range of density profiles associated with nominal dust loading conditions, and with higher dust loading possibly associated with storms, are very benign for the spacecraft during EDL. Further, the major

Table 6. Summary of Ames One-Dimensional Model Results and Comparison to TES Data

Case Description	Ground Diurnal Minimum (°C)	Ground Diurnal Maximum (°C)	TES Diurnal Minimum (°C)	TES Diurnal Maximum (°C)	1-m Diurnal Minimum (°C)	1-m Diurnal Maximum (°C)	Sky Diurnal Minimum (°C)	Sky Diurnal Maximum (°C)
Maximum daytime	−80.9	−2.0	−78 to −74	−22 to −19	−76.8	−18.3	−133.4	−112.6
Minimum nighttime	−87.8	−20.9	−84 to −82	−33 to −29	−83.9	−33.7	−144.5	−123.9
Minimum daytime: Dust storm	−76.4	−51.0	not available	not available	−75.4	−52.7	−97.4	−85.7
Sol 0 maximum daytime	−80.2	−5.1	not available	not available	−76.5	−19.7	−130.0	−110.5
Sol 0 minimum nighttime	−91.8	−14.6	not available	not available	−87.3	−28.0	−135.3	−115.7
Sol 0 nominal	−73.9	−22.4	−82 to −79	−31 to −28	−71.2	−29.9	−129.2	−115.4

effect of circumpolar storm winds, that might be problematic for EDL, should be substantially north of the Phoenix landing latitude. The winds during EDL are expected to be bounded between −10 and +15 m/s in the vertical, with the boundary layer extending to 7- to 8-km altitude, and ±10–15 m/s in the horizontal direction. These magnitudes have been planned for and analysis shows a high probability of landing safely. The spacecraft once landed will experience flows associated with circumpolar systems and with Alba Patera to the south. Expected surface winds during the mission are likely to be <15 m/s, with extended durations of <2 m/s. The winds are not necessarily expected to have a diurnally repeatable pattern since they may be primarily associated with the circumpolar flows. The expected bounds for surface pressure (7–11 mbar) and temperature (185–257 K, covering both surface and near-surface air temperature), over the duration of the mission and over the likely surface A and I, have been used for analysis and test of the spacecraft ability to perform and for planning surface operations. The predicted average visible optical depth is likely to be 0.6 in the beginning of the mission, slowly decreasing to 0.3 at the end of the 90-sol mission. The variability in the TES data over the 3 Mars years examined indicates that 1-sigma high values would be 0.9 and 0.4 at the beginning and end of the nominal mission, respectively. Any dust storms that pass over the lander site will likely have visible optical depths ∼2.0 and last for about 1 sol. However, a worst case storm could last up to 3 sols and/or have a visible optical depth approaching 2.5.

[82] With the complement of instruments that Phoenix will carry, it will be possible to verify if the above estimates are correct. The data acquired during EDL from the inertial mass unit within the spacecraft will be used to back out the actual density that the spacecraft experienced between the top of the sensible atmosphere down to the parachute deploy altitude of ∼13 km. From these data and the surface pressure measured upon landing, the temperature profile can be reconstructed. The Phoenix pressure sensor and temperature sensors [see *Taylor et al.*, 2008] will be able to measure diurnal and seasonal variations. The Solid State Imager (SSI; M. Lemmon, personal communication, 2007) will be able to confirm the local surface albedo as well as provide total visible optical depth measurements as a function of time throughout the mission. The thermal inertia of the local surface will be measured by the Thermal and Electrical Conductivity Probe (TECP; see A. P. Zent et al., The Thermal and Electrical Conductivity Probe for Phoenix, submitted to the *Journal of Geophysical Research*, 2008), which has 4 needles, one of which is heated while others measure the heat conducted through the surface from the first needle. Finally, the winds can be measured occasionally through two methods on the Phoenix spacecraft: via a Telltale [*Taylor et al.*, 2008] that is imaged by the SSI and via the TECP, by holding the probe up in the air and watching the wind's effect on the needles. With these measurements, we expect the Phoenix mission to provide a rich data set from which we will be able to greatly improve our understanding of the summertime northern polar environment.

[83] **Acknowledgments.** This work was carried out at JPL/Caltech through a contract from NASA and at Oregon State University and Southwest Research Institute via contracts from JPL/Caltech.

References

Arvidson, R. E., et al. (2008), Mars Exploration Program 2007 Phoenix landing site selection and characteristics, *J. Geophys. Res.*, *113*, E00A03, doi:10.1029/2007JE003021.

Cantor, B. A., P. B. James, M. Caplinger, and M. J. Wolff (2001), Martian dust storms: 1999 Mars Orbiter Camera Observations, *J. Geophys. Res.*, *106*(E10), 23,653–23,687.

Caughey, S. J., and J. C. Wyngaard (1979), The turbulence kinetic energy budget in convective conditions, *Q. J. R. Meteorol. Soc.*, *105*, 231–239, doi:10.1002/qj.49710544315.

Christensen, P., et al. (1992), Thermal Emission Spectrometer Experiment: Mars Observer Mission, *J. Geophys. Res.*, *97*, 7719–7734.

Clancy, R. T., B. J. Sandor, P. R. Christensen, M. D. Smith, J. C. Pearl, B. J. Conrath, and M. J. Wolff (2000), An intercomparison of ground-based millimeter, MGS TES, and Viking atmospheric temperature measurements: Seasonal and interannual variability of temperatures and dust loading in the global Mars atmosphere, *J. Geophys. Res.*, *105*, 9553–9572, doi:10.1029/1999JE001089.

Clancy, R. T., M. J. Wolff, and P. R. Christensen (2003), Mars aerosol studies with the MGS TES emission phase function observations: Optical depths, particle sizes, and ice cloud types versus latitude and solar longitude, *J. Geophys. Res.*, *108*(E9), 5098, doi:10.1029/2003JE002058.

Golombek, M. P., et al. (2003), Selection of the Mars Exploration Rover landing sites, *J. Geophys. Res.*, *108*(E12), 8072, doi:10.1029/2003JE002074.

Haberle, R. M., M. N. Joshi, J. R. Murphy, J. R. Barnes, J. T. Schofield, G. Wilson, M. Lopez-Valverde, J. L. Hollingsworth, A. F. C. Bridger, and J. Schaffer (1999), General circulation model simulation of the Mars Pathfinder atmospheric structure investigation/meteorology data, *J. Geophys. Res.*, *104*, 8957–8974, doi:10.1029/1998JE900040.

Kaimal, J. C., J. C. Wyngaard, Y. Izumi, and O. R. Cote (1972), Spectral characteristics of surface-layer turbulence, *Q. J. R. Meteorol. Soc.*, *98*, 563–589, doi:10.1002/qj.49709841707.

Kass, D. M., J. T. Schofield, T. I. Michaels, S. C. R. Rafkin, M. I. Richardson, and A. D. Toigo (2003), Analysis of atmospheric mesoscale models for entry, descent, and landing, *J. Geophys. Res.*, *108*(E12), 8090, doi:10.1029/2003JE002065.

Lemmon, M. T., et al. (2004), Atmospheric imaging results from the Mars Exploration Rovers: Spirit and Opportunity, *Science*, *306*, 1753–1756, doi:10.1126/science.1104474.

Malin, M. C., et al. (1992), Mars-Observer camera, *J. Geophys. Res.*, *97*, 7699–7718.

Malin, M. C., et al. (2001), Mars Color Imager (MARCI) on the Mars Climate Orbiter, *J. Geophys. Res.*, *106*, 17,651–17,672, doi:10.1029/1999JE001145.

Malin, M. C., et al. (2007), Context camera investigation on board the Mars Reconnaissance Orbiter, *J. Geophys. Res.*, *112*, E05S04, doi:10.1029/2006JE002808.

Martin, T. Z., N. T. Bridges, and J. R. Murphy (2003), Near-surface temperatures at proposed Mars Exploration Rover landing sites, *J. Geophys. Res.*, *108*(E12), 8089, doi:10.1029/2003JE002063.

McCleese, D. J., J. T. Schofield, F. W. Taylor, S. B. Calcutt, M. C. Foote, D. M. Kass, C. B. Leovy, D. A. Paige, P. L. Read, and R. W. Zurek (2007), Mars Climate Sounder: An investigation of thermal and water vapor structure, dust and condensate distributions in the atmosphere, and energy balance of the polar regions, *J. Geophys. Res.*, *112*, E05S06, doi:10.1029/2006JE002790.

McEwen, A. S., et al. (2007), Mars Reconnaissance Orbiter's High Resolution Imaging Science Experiment (HiRISE), *J. Geophys. Res.*, *112*, E05S02, doi:10.1029/2005JE002605.

Michaels, T. I., and S. C. R. Rafkin (2004), Large-eddy simulation of atmospheric convection on Mars, *Q. J. R. Meteorol. Soc.*, *130*, 1251–1274, doi:10.1256/qj.02.169.

Michaels, T. I., and S. C. R. Rafkin (2008), Meteorological predictions for candidate 2007 Phoenix Mars Lander sites using the Mars Regional Atmospheric Modeling System (MRAMS), *J. Geophys. Res.*, *113*, E00A07, doi:10.1029/2007JE003013.

Putzig, N. E., et al. (2005), Global thermal inertia and surface properties of Mars from the MGS mapping mission, *Icarus*, *173*, 325–341, doi:10.1016/j.icarus.2004.08.017.

Rafkin, S. C. R., and T. I. Michaels (2003), Meteorological predictions for 2003 Mars Exploration Rover high-priority landing sites, *J. Geophys. Res.*, *108*(E12), 8091, doi:10.1029/2002JE002027.

Rafkin, S. C. R., R. M. Haberle, and T. I. Michaels (2001), The Mars Regional Atmospheric Modeling System (MRAMS): Model description and selected simulations, *Icarus*, *151*, 228–256, doi:10.1006/icar.2001.6605.

Rafkin, S. C. R., T. I. Michaels, and R. M. Haberle (2004), Meteorological predictions for the Beagle 2 mission to Mars, *Geophys. Res. Lett.*, *31*, L01703, doi:10.1029/2003GL018966.

Smith, K. S., C. Y. Peng, and A. Behboud (1995), Multibody dynamic simulation of Mars pathfinder entry: Descent and landing, *JPL Doc. D-13298*, Jet Propul. Lab., Pasadena, Calif.

Smith, M. D. (2003), TES limb-geometry observations of aerosols, paper presented at Sixth International Conference on Mars, Jet Propul. Lab., Pasadena, Calif.

Smith, M. D. (2004), Interannual variability in TES atmospheric observations of Mars during 1999–2003, *Icarus*, *167*, 148–165, doi:10.1016/j.icarus.2003.09.010.

Smith, M. D. (2006), TES atmospheric temperature, aerosol, optical depth, and water vapor observations 1999–2004, paper presented at the Second Workshop on Mars Atmospheric Modeling and Observations, Eur. Space Ag., Granada, Spain, 27 Feb.–3 March.

Smith, M. D., M. J. Wolff, N. Spanovich, A. Ghosh, D. Banfield, P. R. Christensen, G. A. Landis, and S. W. Squyres (2006), One Martian year of atmospheric observations using MER Mini-TES, *J. Geophys. Res.*, *111*, E12S13, doi:10.1029/2006JE002770.

Stella, P., R. Ewell, and J. Hoskin (2005), Design and performance of the MER (Mars Exploration Rovers) solar arrays, paper presented at the 31st IEEE Photovoltaic Specialists Conference, Inst. of Electr. and Electron. Eng., Lake Buena Vista, Fla., 3–7 Jan.

Taylor, P. A., D. C. Catling, M. Daly, C. S. Dickinson, H. P. Gunnlaugsson, A.-M. Harri, and C. F. Lange (2008), Temperature, pressure, and wind instrumentation in the Phoenix meteorological package, *J. Geophys. Res.*, *113*, E00A10, doi:10.1029/2007JE003015.

Titus, T. N. (2005), Mars polar cap edges tracked over 3 full Mars years, paper presented at the 36th Lunar and Planetary Science Conference, Lunar and Planet. Inst., League City, Tex., 14–18 March.

Tsuyuki, G., L. Tamppari, T. Martin, and J. Murphy (2007), Development of the surface thermal environment for the Mars Scout Phoenix mission, paper presented at the 37th International Conference on Environmental Systems, Soc. of Automotive Eng., Chicago, Ill., 9–12 July.

Tyler, D., Jr., and J. R. Barnes (2005), A mesoscale model study of summertime atmospheric circulations in the north polar region of Mars, *J. Geophys. Res.*, *110*, E06007, doi:10.1029/2004JE002356.

Tyler, D., Jr., and J. R. Barnes (2006), Mesoscale and LES model simulations of polar meteorology in support of Phoenix, paper presented at the 4th International Conference on Mars Polar Science and Investigation, Lunar and Planet. Inst., Davos, Switzerland, 2–6 Oct.

Tyler, D., Jr., J. R. Barnes, and R. M. Haberle (2002), Simulation of surface meteorology at the Pathfinder and VL1 sites using a Mars mesoscale model, *J. Geophys. Res.*, *107*(E4), 5018, doi:10.1029/2001JE001618.

Tyler, D., Jr., J. R. Barnes, and E. D. Skyllingstad (2008), Mesoscale and large-eddy simulation model studies of the Martian atmosphere in support of Phoenix, *J. Geophys. Res.*, *113*, E00A12, doi:10.1029/2007JE003012.

Wolff, M. J., and R. T. Clancy (2003), Constraints on the size of Martian aerosols from Thermal Emission Spectrometer observations, *J. Geophys. Res.*, *108*(E9), 5097, doi:10.1029/2003JE002057.

Zuber, M. T., et al. (1992), The Mars-Observer Laser Altimeter Investigation, *J. Geophys. Res.*, *97*, 7781–7797.

J. Barnes and D. Tyler Jr., College of Oceanic and Atmospheric Sciences, Oregon State University, 104 COAS Building, Corvallis, OR 97331, USA.

E. Bonfiglio, A. J. Friedson, M. R. Grover, D. Kass, T. Z. Martin, L. K. Tamppari, and G. Tsuyuki, Jet Propulsion Laboratory, California Institute of Technology, 4800 Oak Grove Drive, Pasadena, CA 91109, USA. (leslie.tamppari@jpl.nasa.gov)

B. Cantor, Malin Space Science Systems, Inc., STE 200, 9115 Brown Deer Road, San Diego, CA 92121, USA.

A. Ghosh, Tharsis, Inc., 8227 Ironclad Court, Gaithersburg, MD 20877, USA.

M. Mellon, Laboratory for Atmospheric and Space Physics, University of Colorado, 392 UCB, Boulder, CO 80309, USA.

T. Michaels and S. C. R. Rafkin, Southwest Research Institute, 1050 Walnut Street, #300, Boulder, CO 80302, USA.

J. Murphy, Department of Astronomy, New Mexico State University, MSC 4500, 1320 Frenger, Las Cruces, NM 88003, USA.

M. D. Smith, NASA Goddard Space Flight Center, 8800 Greenbelt Road, Greenbelt, MD 20771, USA.

M. Wolff, Space Science Institute, 4750 Walnut Street, Suite 205, Boulder, CO 80301, USA.